ORIGINAL ARTICLE

A study on beam-to-column moment-resisting timber connections under service load, comparing full-scale connection testing and mock-up frame assembly

Aivars Vilguts[1] · Sveinung Ørjan Nesheim[1] · Haris Stamatopoulos[1] · Kjell Arne Malo[1]

Abstract

A new timber frame structural system consisting of continuous columns, prefabricated hollow box timber decks and beam-to-column moment-resisting connections is investigated. The hollow box timber decks allow long spans with competitive floor height and efficient material consumption. To achieve long spans, semi-rigid connections at the corners of deck elements are used to join the columns to the deck elements. In the present paper, experimental investigations of a semi-rigid moment-resisting connection and a mock-up frame assembly are presented. The semi-rigid connection consists of inclined screwed-in threaded rods and steel coupling parts, connected with friction bolts. Full-scale moment-resisting timber connections were tested under monotonic and cyclic loading to quantify rotational stiffness, energy dissipation and moment resistance. The mock-up frame assembly was tested under cyclic lateral loading and with experimental modal analysis. The lateral stiffness, energy dissipation, rotational stiffness of the connections and the eigen frequencies of the mock-up frame assembly were quantified based on the experimental tests in combination with a Finite Element model, i.e., the model was validated with experimental results from the rotational stiffness tests of the beam-to-column connections. Finally, the structural damping measured with experimental modal analysis was evaluated and compared with FE model using the material damping of timber parts and equivalent viscous damping of the moment-resisting connections.

1 Introduction

1.1 Background

The main aim of the Norwegian research project WOOD-SOL is to develop industrialised structural solutions based on moment-resisting timber frames and hollow box timber decks for urban multi-storey buildings allowing for greater architectural flexibility. The moment-resisting frames, the hollow box timber decks, the moment-resisting connections and the acoustic properties of the buildings are the research objectives of the project. The structural system consists of moment-resisting timber frames with continuous columns and hollow box timber decks connected to columns via semi-rigid beam-to-column connections.

The main purpose of a building's structural system is to carry vertical and lateral loads to the foundation. The type of structural system is chosen taking architectural and structural restrictions into account and a system based on moment-resisting timber frames with semi-rigid beam-to-column connections can be an interesting alternative. Timber frames offer many opportunities such as constructability, low environmental footprint and high strength-to-mass ratio (Gohlich et al. 2018; Kasal et al. 2014). Hollow box timber decks can be very effective floor elements and are further improved when connected by moment-resisting connections to the columns. Malo and Köhler (2013) showed that semi-rigid end restraints of beams can be exploited to achieve enhanced performance against human-induced vibrations and the possibility to increase spans between load bearing structures.

In timber engineering, the connections between structural elements are a crucial factor in the design of the structure. The overall strength and stiffness of the structures will typically be governed to a significant extent by the strength and stiffness of the connections. The most widely used connection types in timber engineering are laterally and axially

✉ Aivars Vilguts
  aivars.vilguts@gmail.com

1   Department of Structural Engineering, Norwegian University of Science and Technology (NTNU), Rich. Birkelandsvei 1A, 7491 Trondheim, Norway

loaded fasteners. Laterally loaded fasteners like dowel-type or bolted-type connections with slotted-in steel plates are commonly used as a connection between two or more structural elements. Dowel-type connections are designed to carry and withstand axial and shear forces. Such connections can be designed to carry bending moments. Solarino et al. (2017) performed experimental tests on typical beam-to-column moment-resisting dowel-type connection. The measured rotational stiffness in the range of $0.1\,M_{max} < M < 0.4\,M_{max}$ was 696 kNm/rad.

Lam et al. (2010) evaluated the performance of moment-resisting bolted timber connections with reinforcing wood screws inserted perpendicular to grain. The rotational stiffness of such a connection ranged from 850 to 2060 kNm/rad. Brandon and Leijten (2014) presented a study of two 3-member densified veneer wood reinforced timber connections with an inter-connecting steel plate used as middle member. Studies have shown that reinforcing dowel-type timber connections with 'densified veneer wood' and using expanded tube fasteners result in connections with superior structural properties compared to all conventional connections. The experimental tests of such a connection showed rotational stiffness of 1000 kNm/rad.

Axially loaded fasteners, like self-tapping screws (STS) or glued-in rods utilise the high axial stiffness of the fasteners. Komatsu et al. (2019) presented an experimental and analytical investigation of beam-to-column moment-resisting connection with STS and steel side plates. The beam-to-column moment-resisting connection showed initial stiffness of 1250 kNm/rad and an average moment resistance of 49.35 kNm. Leimcke et al. (2016) tested beam-to-column moment-resisting connection based on friction damping device and glued-in rods under cyclic loading. The test results showed high-energy dissipation without degradation of the timber beam or column. Andreolli et al. (2011) investigated the mechanical characteristics of moment-resisting connection with glued-in rods and steel end-plates suitable for different configurations of heavy timber frames. Two connection

configurations were tested under monotonic and cyclic loading. The highest recorded rotational stiffness of the connection was approx. 2240 kNm/rad and 460 kNm/rad at failure. Buchanan et al. (2008) developed and showed the conceptual solution for a hybrid beam-column timber connection, based on the combination of post-tensioning and internal dissipaters (e.g. epoxied mild steel bars). The developed beam-to-column connection based on post-tensioning and internal dissipaters demonstrated high-seismic performance and large inelastic displacements (high-ductility demand).

To increase the span length of hollow box timber decks and to satisfy the structural requirements of buildings, the semi-rigid connection stiffness should be sufficient. The research presented in Vilguts et al. (2020) concluded that the connection stiffness required for multi-storey timber buildings with moment-resisting frames as the only lateral load resisting system should be around 10,000–15,000 kNm/rad. The moment-resisting timber connection with screwed-in, inclined threaded rods with wood screw threads and steel coupling parts has been presented in Lied and Nordal (2016) and Vilguts et al. (2018). Based on tests of these connection types, rotational stiffness values up to approx. 8000 kNm/rad can be achieved for two planes of rods. Therefore, the required stiffness values can be achieved with approx. 2–6 rod planes. Finally, moment-resisting timber frames may be used as a primary or secondary stabilising system in timber buildings in combinations with shear walls or truss systems depending on the design requirements, providing additional lateral stiffness to a building or increasing spans between load bearing constructions.

1.2 Outline

In the present paper, the experimental results from full-scale tests of a moment-resisting connection with inclined threaded rods and steel coupling parts are presented. The connections as shown in Fig. 1a were subjected to both cyclic and monotonic loading and the rotational stiffness,

Fig. 1 **a** Moment resisting connection with inclined threaded rods and steel coupling parts comprising of L-profiles interconnected with friction bolts. **b** Mock-up frame assembly, photo: SINTEF/A.-L.Bakken

(a)

(b)
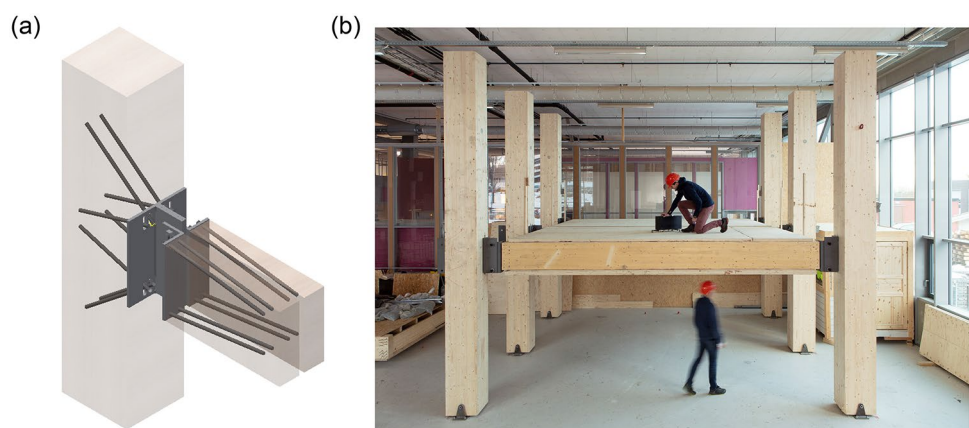
moment resistance and energy dissipation in the low-intensity domain were quantified. The experimental results from monotonic loading tests were compared to an analytical component model (Stamatopoulos and Malo 2020a). Moreover, a mock-up frame assembly with columns and hollow box timber decks connected with the moment-resisting connections, see Fig. 1b, was used to evaluate the properties of the connections in the frame assembly. The frame assembly was subjected to cyclic lateral loading and the lateral stiffness, energy dissipation and rotational stiffness of the connections were evaluated. In addition, the energy dissipation was estimated in the longitudinal and transversal directions of the frame assembly using the modal hammer technique followed by experimental modal analysis. The experimental results from the tests were input to finite element (FE) simulations, where the experimentally measured rotational stiffness and energy dissipation of the beam-to-column connections were used to model the behaviour of the connections in the mock-up frame assembly. Finally, the static and dynamic properties from experimental tests were evaluated and compared with results from FE modelling.

2 Materials and methods

2.1 Moment-resisting connections

2.1.1 Experimental set-up and specimens

Three full-scale moment-resisting timber connections were tested under cyclic loading, to evaluate rotational stiffness and energy dissipation. One out of these three tests was tested until failure to explore the complete behaviour with respect to rotational stiffness and moment resistance. The experimental set-up is shown in Fig. 2 with corresponding pictures in Fig. 3. In total, 3 columns, 2 beams and 3 steel coupling parts were used to assemble the connection specimens.

The beam-to-column moment-resisting connection consists of two timber beams, steel coupling parts and a timber column. The threaded rods at the beam-side were installed with rod-to-grain angle of 10°, while in the column-side 55 and 70° were used, as shown in Fig. 2b. The threaded rods were screwed in predrilled holes with diameter 17 mm. The rods were manufactured with two types of threads at their ends: wood screw threads in one end and M20 metric threads at the other end, as shown in Fig. 4. The inner and outer diameter of the wood screw threads were $d_1 = 16.1$ mm and $d = 22$ mm, respectively. The mean ultimate strength of the rods was $f_{u,mean} = 952$ MPa (Lied and Nordal 2016).

The steel coupling parts at the beam-side and column-side were connected to the rods by use of purpose-made steel washers and M20 nuts, as shown in Fig. 2b. The steel coupling parts

were made from standard L200 × 200 × 16 profiles (strength class S355) with oversized holes, to allow better fitting to the inclined threaded rods. The steel coupling parts were fastened to the column and beams with 5 mm and 20 mm gaps respectively, as shown in Fig. 2b. These intended gaps ensured that the forces were transferred solely by the threaded rods. The beam- and column-side steel coupling parts were connected with two M30 high strength friction bolts of strength class 12.9. The applied pre-stressing torque of the bolts was 2500 Nm. The rod-to-grain angles α_i, embedment lengths of rods l_i, and the free length of the rods $l_{0,i}$ (i.e. the distance between the entrance point on wood and the fixing point in the steel plates) for tests are summarized in Table 1. The values in Table 1 are given for positive moment according to Fig. 2a.

Columns and beams were glued-laminated timber (glulam) elements made from Norway spruce (*Picea abies*) with strength class GL30c according to EN 14080:2013 (European Committee for Standardization 2013) and lamination thickness 45 mm. The cross-sectional dimensions of the columns were 405×450 mm^2 (i.e. block glued glulam), while the beams were 140×405 mm^2, confer Fig. 2a, c. The timber specimens were conditioned at temperature of 20 ºC and 65% relative humidity, resulting in approximately 12% moisture content in the wood.

The supports at both ends of the column were pinned. To prevent splitting perpendicular to grain, steel brackets were mounted at both supports, as shown in Fig. 3 (a). The point loading was applied on the beams by a clamp of two aluminium profiles (Fig. 3 (c)), which allowed both positive and negative point loading.

The deformation in beams, column and steel coupling parts was measured by a total of 12 displacement transducers (LVDTs), confer Fig. 2d. The relative horizontal deformation between the column and the beams was measured with four LVDTs (TD1, TD2, TD3, TD4). Four LVDTs measured the relative horizontal deformation between the column and the steel coupling parts at column-side (CD1, CD2, CD3, CD4), and four LVDTs measured the relative horizontal deformation between the beam and the steel coupler at beam-side (BD1, BD2, BD3, BD4). The total rotation of connection, column and beam was calculated accordingly:

$$\theta_{y,t} = \frac{\left(\frac{\delta_{TD1}+\delta_{TD2}}{2}\right) - \left(\frac{\delta_{TD3}+\delta_{TD4}}{2}\right)}{z_t} \tag{1}$$

$$\theta_{y,c} = \frac{\left(\frac{\delta_{CD1}+\delta_{CD2}}{2}\right) - \left(\frac{\delta_{CD3}+\delta_{CD4}}{2}\right)}{z_c} \tag{2}$$
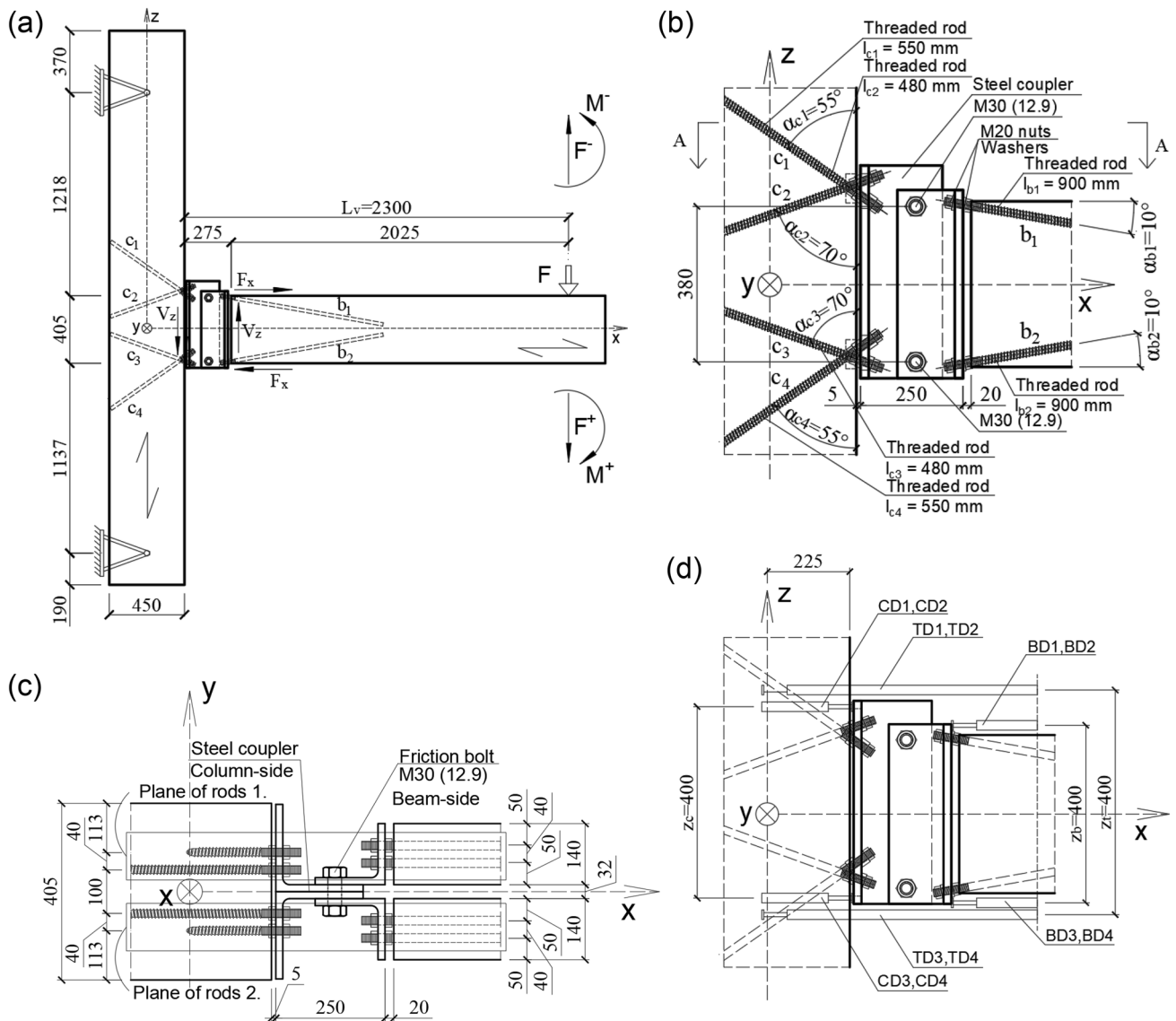
Fig. 2 Experimental set-up: **a** beam-to-column moment-resisting connection, **b** technical layout of the connection, **c** section A-A, **d** location of instrumentation

$$\theta_{y,b} = \frac{\left(\frac{\delta_{BD1}+\delta_{BD2}}{2}\right) - \left(\frac{\delta_{BD3}+\delta_{BD4}}{2}\right)}{z_b} \tag{3}$$

where z_t, z_c, z_b− are the lever arms between LVDTs for the total rotation of connection, column and beam, see Fig. 2 and δ_i− are the measured relative displacements.

2.1.2 Loading protocol

In total, four loading protocols were applied, as shown in Table 2:

- Fully reversed cyclic loading in the range of + 30 to − 30 kNm. The cyclic rotational stiffness $K_{\theta,cyc}$ was obtained by fitting a straight line to the hysteresis loops giving a representative stiffness for a connection subjected to cyclic alternate loading (typical in structures subjected to vibration). The area enclosed in each hysteresis loop is the energy dissipation per cycle E_d. The load was applied with a quasi-static rate with a frequency of $f = 0.008$ Hz. The range of the applied moment (± 30kNm) was considered as a representative service load and approximated as 40% of the estimated moment resistance according to EN 26891:1991 (European Committee for Standardization 1991).
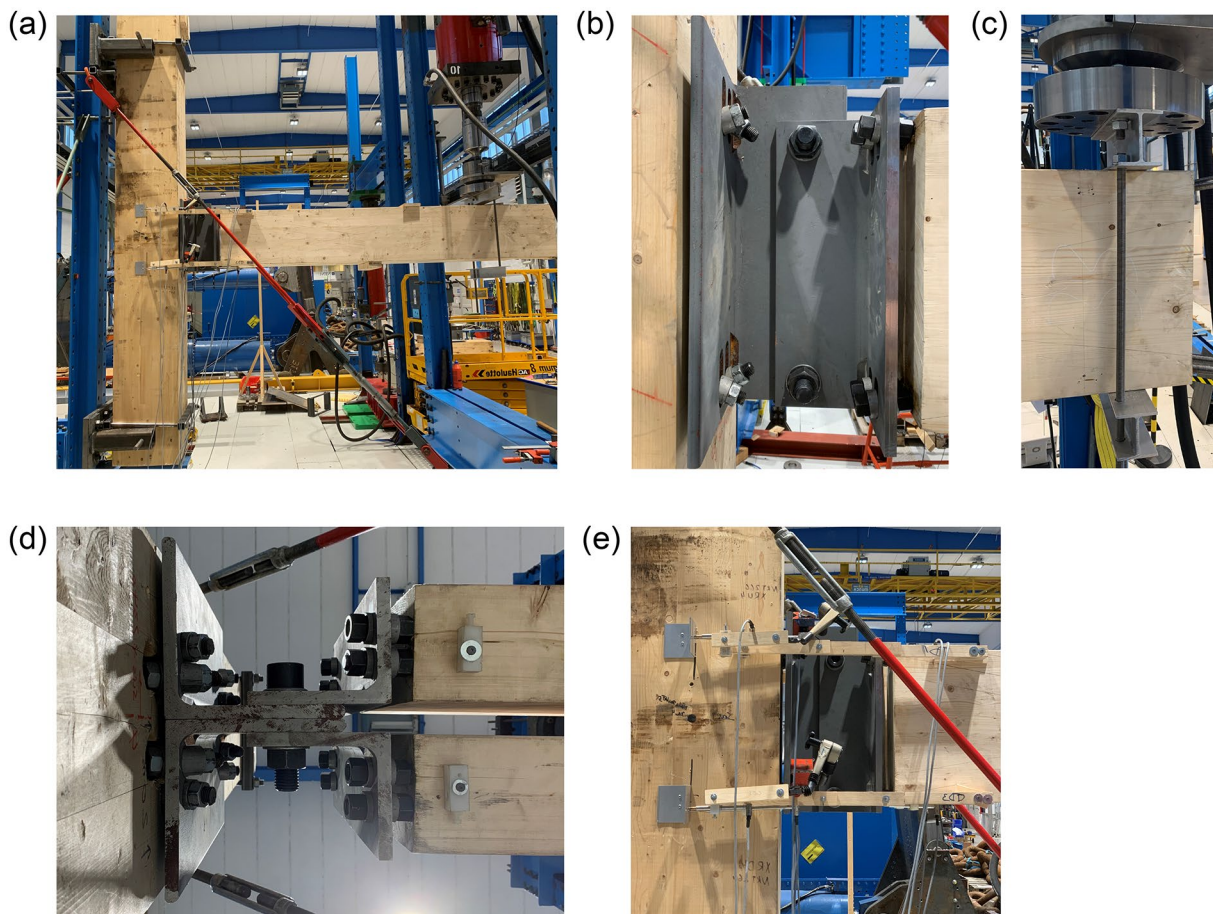
Fig. 3 Detailed experimental set-up: **a** experimental set-up, **b** steel coupling part, **c** load application, **d** bottom-view of the connection, **e** locations of LVDTs

Fig. 4 Threaded rod

Wood screw-thread $d_1 = 16.1$ and $d = 22$ mm.   Metric thread M20

Table 1 Parameters for experimental set-up according to Fig. 2

$\alpha_{c1} = \alpha_{c4}$ (deg)	$\alpha_{c2} = \alpha_{c3}$ (deg)	$\alpha_{b1} = \alpha_{b2}$ (deg)	$l_{c1} = l_{c4}$ (mm)	$l_{c2} = l_{c3}$ (mm)	$l_{b1} = l_{b2}$ (mm)	$l_{0,c1}$ [a] (mm)	$l_{0,c2}$ [a] (mm)	$l_{0,c3}$ [a] (mm)	$l_{0,c4}$ [a] (mm)	$l_{0,b1}$ [a] (mm)	$l_{0,c2}$ [a] (mm)	z (mm)
55	70	10	550	480	850	65	55	40	45	45	25	400

[a]$l_{0,c1} \neq l_{0,c4}$, $l_{0,c2} \neq l_{0,c3}$ and $l_{0,b1} \neq l_{0,b2}$ despite geometrical symmetry: the tensile forces at the top edge are transferred by contact between fixing washers and the interior surface of steel plates, while in the bottom edge the compressive forces are transferred by contact of fixing washers and the exterior surface of steel plates

- Cyclic loading with positive moment ranging from $+7.5$ to $+30$ kNm and cyclic loading with negative moment ranging from -7.5 to -30 kNm. These loading schemes do not give alternating signs, that is, the moment does not go through zero moment. The cyclic rotational stiffness and the energy dissipation are determined for each side separately. The load was applied with a quasi-static rate with a frequency of $f = 0.015$ Hz.

Table 2 Imposed moment vs rotation for the moment-resisting beam-to-column connections according to the various loading schemes

Loading scheme	Measured response
1.	
2.	
3.	
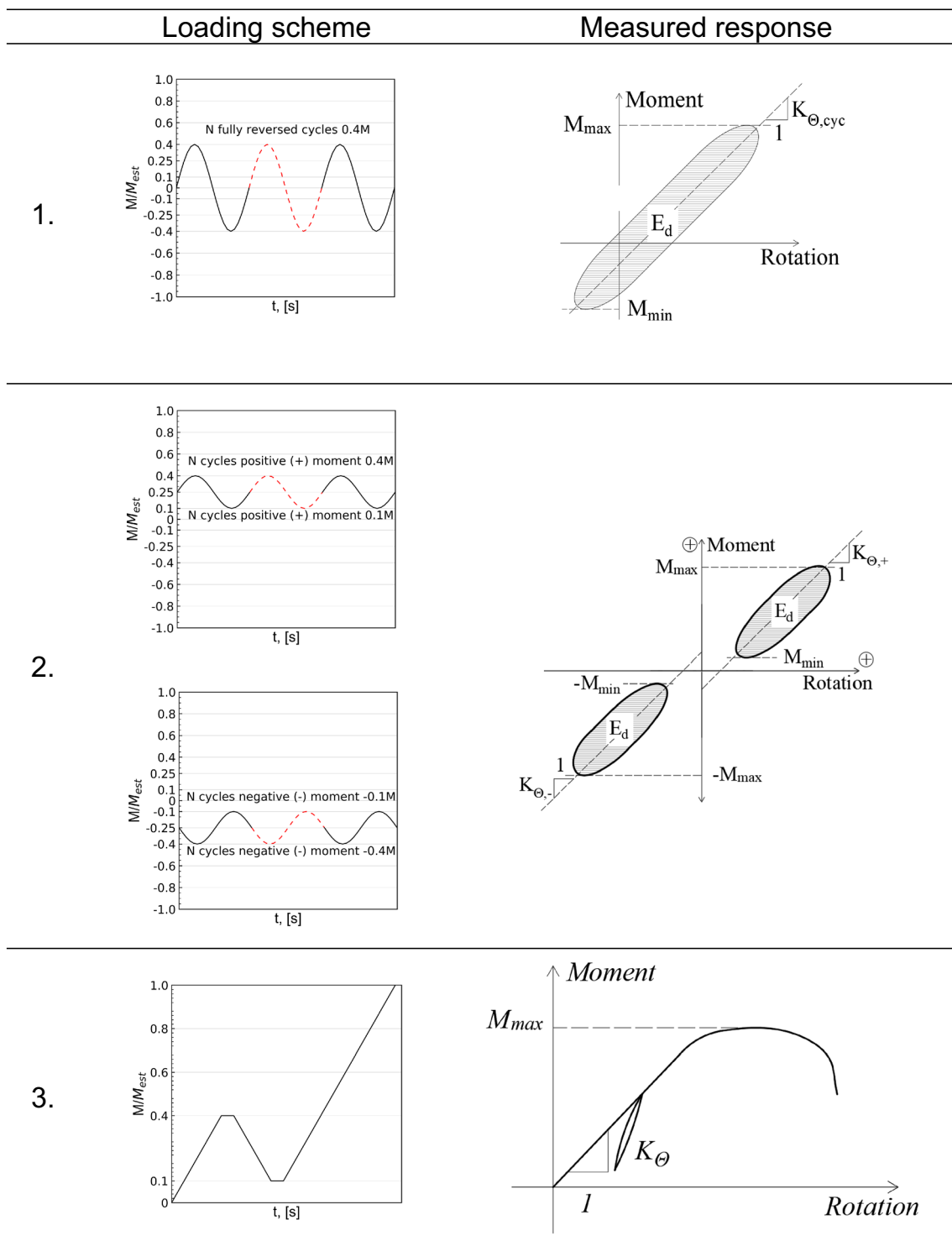
- Monotonic loading until failure according to EN 26891:1991 (European Committee for Standardization 1991).

All three columns with one double beam were tested according to the testing protocol in the following order: cyclic loading with positive moment, cyclic loading with negative moment and fully reversed cyclic loading. Exception was the third column, where after the cyclic testing

protocol described above, the specimen was subjected to monotonic loading until failure.

2.1.3 Equivalent viscous damping

To quantify energy dissipation in the connection subjected to cyclic loading, the equivalent viscous damping ratio is estimated according to Eq. (4) (Chopra 2012):

$$\xi_{eq} = \frac{1}{4\pi} \frac{E_d}{\Delta E_{el}} \tag{4}$$

where E_d is the dissipated energy per cycle and $\Delta E_{el}-$ is the corresponding change in elastic energy per cycle. The dissipated energy E_d per cycle can be found from the measured enclosed area in the hysteresis loop, visualised in Table 2. The maximum elastic change ΔE_{el} during a cycle is:

- In case of moment-rotation:

$$\Delta E_{el} = \frac{1}{2} \frac{M_a^2}{K_{\theta,cyc}} \tag{5}$$

- In case of force–displacement:

$$\Delta E_{el} = \frac{1}{2} \frac{F_a^2}{K_{ax,cyc}} \tag{6}$$

where $M_a = 1/2 \times (M_{max} - M_{min})$ and $F_a = 1/2 \times (F_{max} - F_{min})$, M_{max} and $M_{min}-$ are the maximum and minimum moments in the hysteresis loop, F_{max} and $F_{min}-$ are the maximum and minimum applied forces in the hysteresis loop, $K_{\theta,cyc}, K_{ax,cyc}-$ are the linear stiffnesses obtained by fitting a straight line to all points in the hysteresis loop, using the method of least squares.

2.1.4 Analytical methods

2.1.4.1 Rotational stiffness of connection
The analytical model proposed in Stamatopoulos and Malo (2020a) is used in the present paper to calculate the rotational stiffness and resistance of the connection. The analytical model considers the connection in three separate parts: column-side, beam-side and steel coupling part.

The horizontal force component F_x is obtained by moment equilibrium, as shown in Fig. 2:

$$F_x = \frac{M}{z} \tag{7}$$

where $M-$ is the moment acting on the connection and $z-$ is the lever arm of the connection.

The rotational stiffness about y-axis of the connection at the column-side is obtained using the following equation (Stamatopoulos and Malo 2020a):

$$K_{\theta,y,c} = \frac{M_y}{\theta_{y,c}} = \frac{z_c^2}{\left(S_{xx,c}^{(c1-c2)} + S_{xx,c}^{(c3-c4)}\right) + \left(S_{xz,c}^{(c3-c4)} - S_{xz,c}^{(c1-c2)}\right) \times \frac{z_c}{2 \times L_v}} \tag{8}$$

$$S_{xx,c}^{(c1-c2)} = \frac{\cos^2\alpha_{c1}/K_{ax,c2} + \cos^2\alpha_{c2}/K_{ax,c1}}{\left(\cos\alpha_{c1} \times \sin\alpha_{c2} + \cos\alpha_{c2} \times \sin\alpha_{c1}\right)^2} \tag{9}$$

$$S_{xx,c}^{(c3-c4)} = \frac{\cos^2\alpha_{c3}/K_{ax,c4} + \cos^2\alpha_{c4}/K_{ax,c3}}{\left(\cos\alpha_{c3} \times \sin\alpha_{c4} + \cos\alpha_{c4} \times \sin\alpha_{c3}\right)^2} \tag{10}$$

$$S_{xz,c}^{(c1-c2)} = \frac{\cos\alpha_{c1} \times \sin\alpha_{c1}/K_{ax,c2} - \cos\alpha_{c2} \times \sin\alpha_{c2}/K_{ax,c1}}{\left(\cos\alpha_{c1} \times \sin\alpha_{c2} + \cos\alpha_{c2} \times \sin\alpha_1\right)^2} \tag{11}$$

$$S_{xz,c}^{(c3-c4)} = \frac{\cos\alpha_{c3} \times \sin\alpha_{c3}/K_{ax,c4} - \cos\alpha_{c4} \times \sin\alpha_{c4}/K_{ax,c3}}{\left(\cos\alpha_{c3} \times \sin\alpha_{c4} + \cos\alpha_{c4} \times \sin\alpha_{c3}\right)^2} \tag{12}$$

where $K_{ax,c1}, K_{ax,c2}, K_{ax,c3}, K_{ax,c4}$ $K_{ax,j}$ are the axial stiffness of rods c_1-c_4 (see Sect. 2.1.4.3), z_c- is the lever arm between threaded rods at column-side, $L_v = M/F-$ (see Fig. 2a) is denoted as the shear length and $\cos\alpha-$ and $\sin\alpha-$ are the angle between the grain and threaded rods (see Fig. 2b).

The rotational stiffness about y-axis of the connection at the beam-side is given by the following equation (Stamatopoulos and Malo 2020a):

$$K_{\theta,y,b} = \frac{M_y}{\theta_{y,b}} = \frac{z_b^2}{\left(S_{xx,b1} + S_{xx,b2}\right) + \left(S_{xz,b2} - S_{xz,b1}\right) \times \frac{z_b}{2 \times L_v}} \tag{13}$$

$$S_{xx,b1} = \frac{\sin\alpha_{b1}{}^2}{K_{v,b1}} + \frac{\cos\alpha_{b1}{}^2}{K_{ax,b1}} \tag{14}$$

$$S_{xx,b2} = \frac{\sin\alpha_{b2}{}^2}{K_{v,b2}} + \frac{\cos\alpha_{b2}{}^2}{K_{ax,b2}} \tag{15}$$

$$S_{xz,b1} = \sin\alpha_{b1} \times \cos\alpha_{b1} \times \left(\frac{1}{K_{v,b1}} - \frac{1}{K_{ax,b1}}\right) \tag{16}$$

$$S_{xz,b2} = \sin\alpha_{b2} \times \cos\alpha_{b2} \times \left(\frac{1}{K_{ax,b2}} - \frac{1}{K_{v,b2}}\right) \tag{17}$$

where $K_{ax,b1}, K_{ax,b2}, K_{v,b1}, K_{v,b2}$ are the axial and lateral stiffness of threaded rods (see Sect. 2.1.4.3), z_b- is the lever arm between threaded rods at beam-side.

The steel connector has coupling parts both at the column- and beam-side, which are inter-connected by friction bolts. The rotational stiffness of the steel connector can be

measured or derived from FE model, see Appendix A in Electronic Supplementary Information.

The total rotational stiffness of the connection can be calculated according to Eq. (18):

$$K_{\theta,y} = \left(\frac{1}{K_{\theta,c}} + \frac{1}{K_{\theta,b}} + \frac{1}{K_{\theta,con}} \right)^{-1} \tag{18}$$

2.1.4.2 Capacity of threaded rods and column The threaded rods are mainly axially loaded and the axial capacity per threaded rod is given by the following equation:

$$F_{ax,R} = \frac{n_{ef}}{n} \times \min \begin{cases} F_{ax,a,R} \\ F_{tens,R} \end{cases} \tag{19}$$

where $n_{ef} = n^{0.9}$ – is the effective number of threaded rods acting together according to EN1995-1–1 (European Committee for Standardization 2010) and $F_{tens,R} = A_s \times f_{u,mean}$ is the tensile capacity of each rod.

On the column-side, the axial forces in each rod can be estimated according to Eqs. (20–23) (Stamatopoulos and Malo 2020a):

$$F_{ax,c1} = \frac{1}{n} \times \frac{\cos\alpha_{c2} + \sin\alpha_{c2} \times \frac{z_c}{2 \times L_v}}{\cos\alpha_{c1} \times \sin\alpha_{c2} + \cos\alpha_{c2} \times \sin\alpha_{c1}} \times \frac{M}{z_c} \tag{20}$$

$$F_{ax,c2} = \frac{1}{n} \times \frac{\cos\alpha_{c1} - \sin\alpha_{c1} \times \frac{z_c}{2 \times L_v}}{\cos\alpha_{c1} \times \sin\alpha_{c2} + \cos\alpha_{c2} \times \sin\alpha_{c1}} \times \frac{M}{z_c} \tag{21}$$

$$F_{ax,c3} = -\frac{1}{n} \times \frac{\cos\alpha_{c4} - \sin\alpha_{c4} \times \frac{z_c}{2 \times L_v}}{\cos\alpha_{c3} \times \sin\alpha_{c4} + \cos\alpha_{c4} \times \sin\alpha_{c3}} \times \frac{M}{z_c} \tag{22}$$

$$F_{ax,c4} = -\frac{1}{n} \times \frac{\cos\alpha_{c3} + \sin\alpha_{c3} \times \frac{z_c}{2 \times L_v}}{\cos\alpha_{c3} \times \sin\alpha_{c4} + \cos\alpha_{c4} \times \sin\alpha_{c3}} \times \frac{M}{z_c} \tag{23}$$

On the beam-side, the axial forces in each rod can be estimated according to Eqs. (24) and (25) (Stamatopoulos and Malo 2020a):

$$F_{ax,b1} = \frac{1}{n} \times \left(\cos\alpha_{b1} + \sin\alpha_{b1} \times \frac{z}{2 \times L_v} \right) \times \frac{M}{z} \tag{24}$$

$$F_{ax,b2} = -\frac{1}{n} \times \left(\cos\alpha_{b2} + \sin\alpha_{b2} \times \frac{z}{2 \times L_v} \right) \times \frac{M}{z} \tag{25}$$

2.1.4.3 Analytical predictions of axial and lateral stiffness and capacity of screwed-in threaded rods The axial stiffness of threaded rod is one of the most important parameters. The

withdrawal stiffness of threaded rods can be approximated by Eqs. (26) and (27) (Stamatopoulos and Malo 2020b):

$$K_{ser,ax} \approx \frac{50000 \times \left(\frac{d}{20} \right)^2 \times \left(\frac{\rho_m}{470} \right)^2 \times k_{lenght,K}}{0.40 \times \cos^{2.3}\alpha + \sin^{2.3}\alpha} \tag{26}$$

$$k_{lenght,K} = \min \left[\left(\frac{l}{300} \right)^{0.75}, 1.0 \right] \tag{27}$$

where d– is the outer-thread diameter of the rod in mm, ρ_m– is the wood density in kg/m³, α– is the rod-to-grain angle and l– is the embedment length in mm.

The axial stiffness of the free part (non-embedded) of the threaded rod is given by the following equation:

$$K_{ax,l0} = A_s \times E_s / l_0 \tag{28}$$

where $A_s = \pi \times d_1^2 / 4$; $E_s = 210,000$ MPa, d_1– is the inner-diameter of threaded rod, l_0– is the free length of the rod not embedded in timber (i.e. the length between the entrance point in wood and the fastening point in the steel coupling parts).

The total axial stiffness of the threaded rods is given by the following equation:

$$K_{ser,ax,tot} = \frac{K_{ser,ax} \times K_{ax,l0}}{K_{ser,ax} + K_{ax,l0}} \tag{29}$$

The lateral stiffness of a threaded rod subjected to lateral loading depends on the rotation of the end of the rod at the connecting point to the steel coupling part (Stamatopoulos and Malo 2020a). For fixed end, the following expression can be used:

$$K_{ser,v,tot} = \frac{3 \times m \times k_v \times l_{ch} \times (\lambda_0 + m)}{\lambda_0^4 + 4 \times \lambda_0^3 \times m + 6 \times \lambda_0^2 \times m + 6 \times \lambda_0 \times m + 3 \times m^2} \tag{30}$$

where $k_v \approx 300$ N/mm² is the foundation modulus of timber (Qazi 2020), $m = d_{net}^4 / d_1^4$ $\lambda_0 = l_0 / l_c$, $l_{ch} = \sqrt[4]{4 \times E_s \times I_s / k_v}$. The flexural stiffness of the embedded part screw is $E_s \times I_s = E_s \times \pi \times d_1^4 / 64$, $d_{net} = 0.9 \times 20 = 18$ mm is the diameter of the non-embedded part.

A simplified expression, derived in (Stamatopoulos and Malo 2020b), can be used to estimate mean withdrawal capacity of threaded rods:

$$F_{ax,a,R} \approx 15.0 \times d \times l \times \left(\frac{\rho_m}{470} \right) \tag{31}$$

2.2 Mock-up frame assembly

2.2.1 Experimental set-up and specimens

The mock-up frame assembly shown in Fig. 5 was used to evaluate the properties of connections in moment-resisting frame. The mock-up frame assembly consisted of six glulam columns and two hollow 4.7 m long box timber deck elements. The connections were similar to those presented in Sect. 2.1, as shown in Fig. 5b, c. A cross-section of two parallel floor elements in direction of the span is shown

in Fig. 5d. Each of the deck elements consisted of two external parallel glulam beams (1) of GL30c with cross section of 140×405 mm^2 and three internal glulam beams (2) of GL28c with cross section of 66×405 mm^2. The top (3) and bottom (4) flanges were made from Kerto-Q LVL plates with thickness of 43 mm and 61 mm, respectively. The elastic material properties are given in Table 3.

The flange plates (Kerto-Q) were glued to beams with phenol-resorcinol adhesive and therefore rigid behaviour at the interface was assumed. The deck elements were
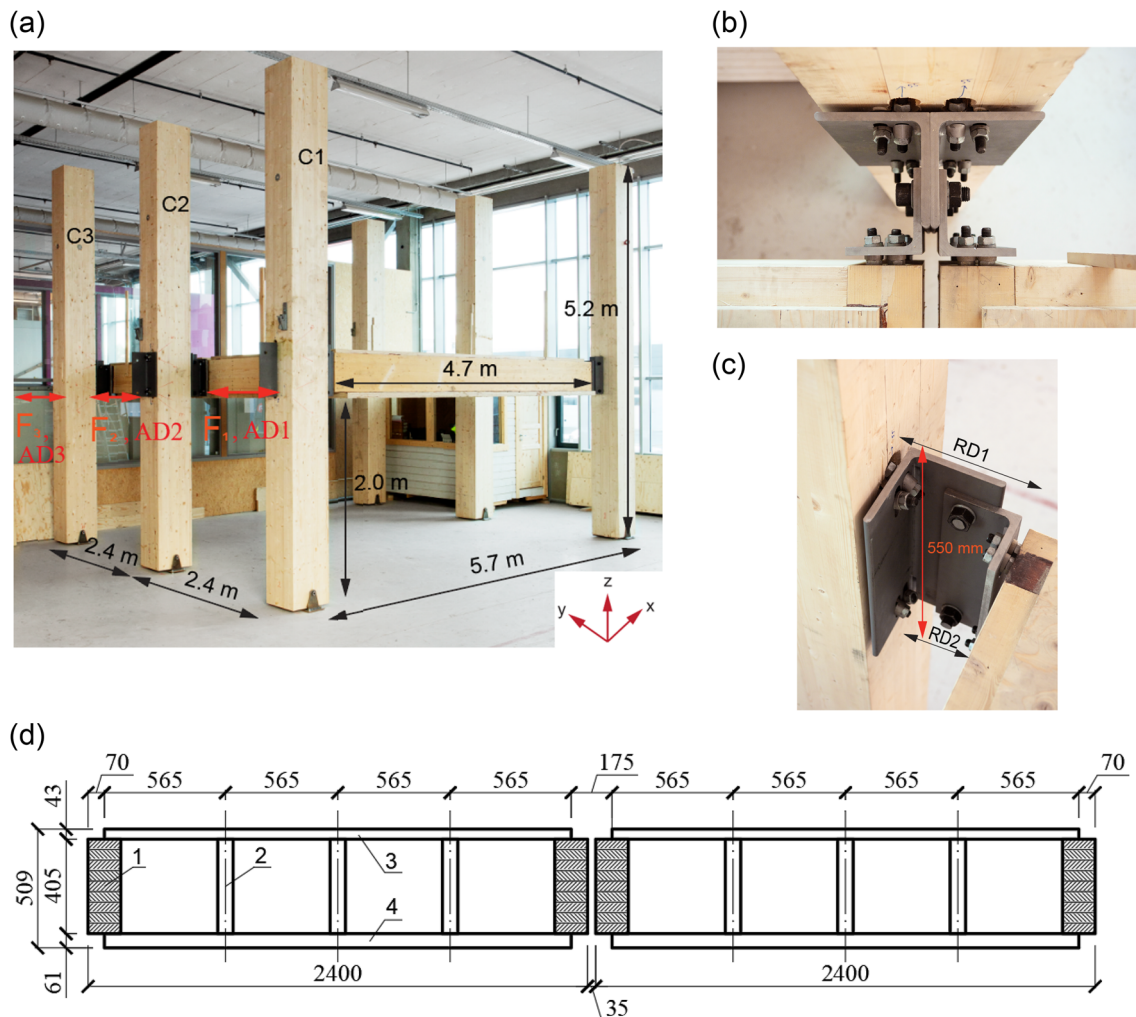

Fig. 5 Mock-up frame assembly set-up. **a** Overview of the construction, **b** connection between floors and centre columns (C$_2$), **c** connection between floors and edge columns (C$_1$ and C$_3$), **d** cross-section of the floor elements. Photo **a–c**: SINTEF/A.-L.Bakken

Table 3 Material properties (Kristoffersen and Bjørge 2017)		P, [kg/m^3]	E_L, [MPa]	E_t, [MPa]	E_R, [MPa]	G_{LR}, [MPa]	G_{LT}, [MPa]	G_{RT}, [MPa]
	GL30c	430	13,000	300	300	600	600	30
	LVL (Kerto-Q)	510	10,500	2400	130	600	120	22

installed to the columns with the bottom flange 2 m above the floor level.

The columns were 5.2 m high with a block-glued cross-section of 405×450 mm². The columns used in this set-up were the same columns as used for the beam-to-column moment-resisting tests described in Sect. 2.1. The columns were installed on the concrete floor with brackets, which allowed rotation about y-axis, as shown in Fig. 5a, that is, the connections to the floor were pinned about the y-axis.

The hollow box decks elements were connected to the columns with the moment-resisting connections described in Sect. 2.1. Two M30 high strength friction bolts (grade 12.9) with applied prestressing torque on the bolts of 2500 Nm were used. Both floor elements shared the central column (C_2) with the double-sided connection shown in Fig. 5b, while the connections to the corner columns were a single-sided version of the same connection, as shown in Fig. 5c.

2.2.2 Loading protocol and instrumentation

To evaluate lateral stiffness, energy dissipation and some dynamic properties of the frame assembly, the following tests were performed:

1. Cyclic loading (loading–unloading) from 0 to $+11/12$ kN. The load was applied two meters above the concrete floor. This loading was applied on each one of the columns (C_1, C_2, C_3) separately, that is, three test series were performed in total. The load was applied with a quasi-static rate with a frequency of $f = 0.02$ Hz.

2. Experimental modal analysis (EMA), by use of the roving hammer technique using one reference accelerometer and a defined grid of hammering points. The impact loads were imposed at the level of the moment-resisting connections as shown in Fig. 6b; in the direction of moment-resisting connections (x-axis), and in the transversal direction (y-axis). An impact hammer with a soft rubber cap was used to excite the structure. Two impacts at each point of the grid were executed, recorded and averaged. The experimental modal analysis was limited to the two horizontal directions.

The lateral deformations of the prototype frame construction were measured by a total of 9 LVDTs. Three LVDTs measured the absolute displacements (x-axis) of the columns (C_1, C_2, C_3) two meters from the concrete floor (AD1, AD2, AD3). Two LVDTs for each column as illustrated in Fig. 5c for column C_1 with RD1 and RD2 were used to measure the relative displacements between the columns and floor elements at the top and bottom levels of the moment-resisting connections, which allowed to determine their rotations. Additionally, for column C_2, relative displacements were measured by LVDTs RD3 and RD4 and for column C_3, relative displacements were measured by LVDTs RD5 and RD6.

2.2.3 Finite element analysis

Finite Element analysis of frame assembly was carried out by SAP2000 Finite Element software (SAP 2000; Wilson and Habibullah 1997), where the rotational stiffness of moment-resisting connections on the mock-up frame
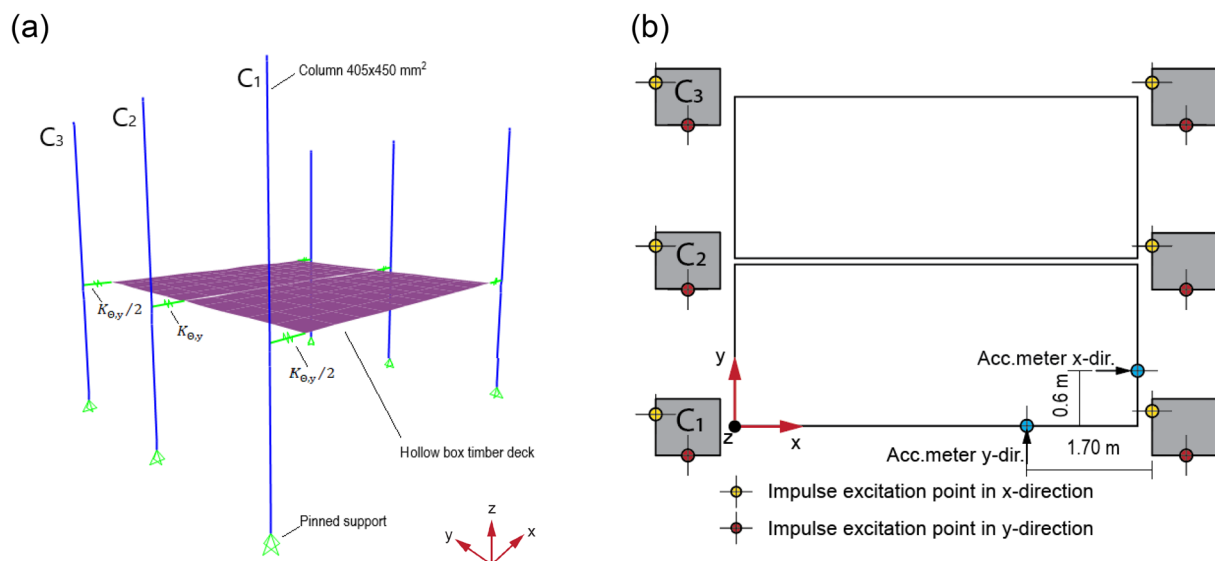

Fig. 6 **a** 3D FE model of frame structure, **b** horizontal cross-section of the frame assembly showing the locations of accelerometers and excitation points

assembly is the emphasized issue. The obtained results are compared to the experimental tests. The layout of the 3D frame structure is shown in Fig. 6a.

The glulam columns were modelled with linear elastic beam elements with mean elastic moduli equal to: $E_{0,mean,c} = 13,000$ MPa and $G_{mean,c} = 650$ MPa for GL30c according to EN14080:2013 (European Committee for Standardization 2013), see Table 3. The floor elements were modelled as thick shell elements with effective bending stiffness of $EI_{f,longitudinal} = 6.7 \times 10^{13}$ N × mm^2 in the longitudinal x-direction (Conta and Homb 2020) and $EI_{f,transversal} = 4 \times 10^{13}$ N × mm^2 in the transversal y-direction (Kristoffersen and Bjørge 2017). These effective bending stiffness values in longitudinal and transversal directions were measured experimentally.

The moment-resisting connections between columns and floor elements were modelled as semi-rigid with respect to the rotational degrees of freedom (DOF) about x- and y-axis. Linear-elastic rotational springs with spring constants $K_{\theta,x}$ and $K_{\theta,y}$ represented the moment-resisting connections. The translational DOFs were fixed between columns and decks in all directions, while the rotation about z-axis was released (pinned). The rotational stiffness values $K_{\Theta,y}$ used for FE analysis were taken from the experimental tests of the moment-resisting connections. For the centric columns (C_2), the rotational stiffness was $K_{\theta,y}$, but for the connections at the corner columns (C_1 and C_3) $K_{\theta,y}/2$ was used. The connections for the C_2 columns consist of the double amount of threaded rods and steel coupling parts compared to the connections at the corner columns.

2.2.4 Analytical predictions of connection stiffness about x-axis

The rotational stiffness about x-axis $K_{\theta,x}$ was estimated from the following expressions as the total connection rotational stiffness, column-side stiffness and beam-side stiffness, respectively:

$$K_{\theta,x} = \frac{K_{\theta,x,c} \times K_{\theta,x,b}}{K_{\theta,x,c} + K_{\theta,x,b}} \qquad (32)$$

$$K_{\theta,x,c} = \frac{M_x}{\theta_{x,c}} = z_{x,c}^2 \times \left(\frac{1}{K_{v,y,c}} + \frac{1}{K_{v,y,c}} \right)^{-1} \qquad (33)$$

$$K_{\theta,x,b} = \frac{M_x}{\theta_{x,b}} = z_{x,b}^2 \times \left(\frac{1}{K_{v,y,b}} + \frac{1}{K_{v,y,b}} \right)^{-1} \qquad (34)$$

where $K_{v,y,c}, K_{v,y,b}$ – are the lateral stiffness of threaded rods (see Sect. 2.1.4.3) and $z_{x,c}, z_{x,b}$ – are the lever arms between threaded rods in column and beam, respectively.

2.2.5 Free damped vibrations of mock-up frame assembly

One major objective in the present research was to explore possible prediction of structural damping based on knowledge of mass, stiffness and damping characteristics of each of the components constituting a complete structure. The mock-up frame assembly, see Fig. 1b, was modelled with the FE model shown in Fig. 6a. The following values (in parenthesis) were used for the material damping in the various components; timber columns (0.5%) (Labonnote et al. 2013), hollow box timber decks (1.5%) (Conta and Homb 2020) and the stiffness and mass were modelled by their representative tabulated mean values. The moment-resisting connections were modelled as linear-elastic rotational springs with the average values of spring stiffness from the cyclic tests of the connections. The equivalent viscous damping of the connections in the FE model was modelled by the rotational damping coefficient (c) as stiffness-proportional damping (Chopra 2012):

$$c = \beta \times K_{\theta,y} \qquad (35)$$

where $\beta = 2\xi_{eq}/\omega_{n,x}, \xi_{eq}$ – is the experimentally measured equivalent viscous damping for the connections (equivalent viscous damping assumed equal for all the connection in FE model), and $\omega_{n,x} = 2\pi \times f_{n,x}$, $f_{n,x}$ – is the undamped fundamental eigenfrequency obtained from FE simulations along x-direction. In calculations of damping coefficient (c), the rotational stiffness of connections on centric columns (C_2) $K_{\theta,y}$ was taken from cyclic experimental tests of the moment-resisting connections, while the rotational stiffness on the corner columns (C_1 and C_3) was taken as $K_{\theta,y}/2$.

Using the FE model and initial conditions (applied displacement on columns along x-axis), a damped free vibration was obtained in the x-direction of the mock-up frame assembly. The structural damping from the damped simulation was estimated using the method with logarithmic decrement, leading to Eq. (36) (Chopra 2012):

$$\xi = \frac{1}{2\pi j} \ln \frac{u_i}{u_{i+j}} \qquad (36)$$

where j – is the number of cycles for evaluation, u_i – is the maximum displacement of i-th cycle and u_{i+j} – is the (decreased) displacement of $(i + j)$-th cycle.

From the free vibrational response of the FE model by applying the material and connection mechanical properties, the vibrational frequency and the structural damping for the structure were determined.

3 Results and discussion

3.1 Moment-resisting connection

3.1.1 Cyclic loading tests

Initially, cyclic tests were performed on the moment-resisting connections using the loading protocols presented in Sect. 2.1.2. For each cyclic loading case, 10 cycles were performed. The experimentally recorded moment-rotation hysteresis loops for each specimen are shown in Fig. 7, where the first column gives the total rotational stiffness for the test set-ups, while the second and third columns visualise the contributions from beam-side and column-side, respectively. Table 4 summarizes the experimentally recorded cyclic stiffness values, the (average) energy dissipation per cycle and the equivalent viscous damping ratios according to Eq. (5) for the connection and for each part separately.

The mean rotational stiffness measured for fully reversed cyclic loading $K_{\theta,cyc} = 4175$ kNm/rad is slightly lower compared to mean values of the rotational stiffness for positive moment ($K_{\theta,+} = 4900$ kNm/rad) and negative moment ($K_{\theta,-} = 4480$ kNm/rad). Furthermore, the measured stiffness values from monotonic loading (4761 kNm/rad) are quite similar to all the values recorded from the cyclic tests. The mean rotational stiffness on the column-side connection ranges from 8341 to 8815 kNm/rad and on the beam-side connection, the mean rotational stiffness ranges from 34,367 to 41,939 kNm/rad.

The mean equivalent damping ratios are similar for fully reversed loading (4.2%), positive moment (4.7%) and negative moment (4.9%) with variability coefficient of 13.4%, 18.9% and 11.4%, respectively. The mean equivalent viscous damping ratios for the beam-side connection are approximately two times higher compared to column-side, both for fully reversed loading (5.7% vs 2.6%), cyclic loading under positive moment (6.3% vs 3.8%) and cyclic loading under negative moment (6.6% vs 2.4%). This finding may be related to the fact that more threaded rods are used on the beam-side possibly resulting in larger energy dissipation.

3.2 Mock-up frame assembly

3.2.1 Cyclic loading tests

The experimental results from cyclic loading tests are given in Fig. 8 in terms of force–displacement hysteresis loops for each loading point and displacement measurement. The displacements in x-direction were monitored by the LVDTs attached to the columns C_1, C_2 and C_3, as shown in Fig. 5a. Consequently, Fig. 8 can be interpreted as a graphical 3×3 stiffness matrix. As it may be observed, the off-diagonal elements are fairly symmetric and indicate the degree of coupling effects between the three columns. The corresponding
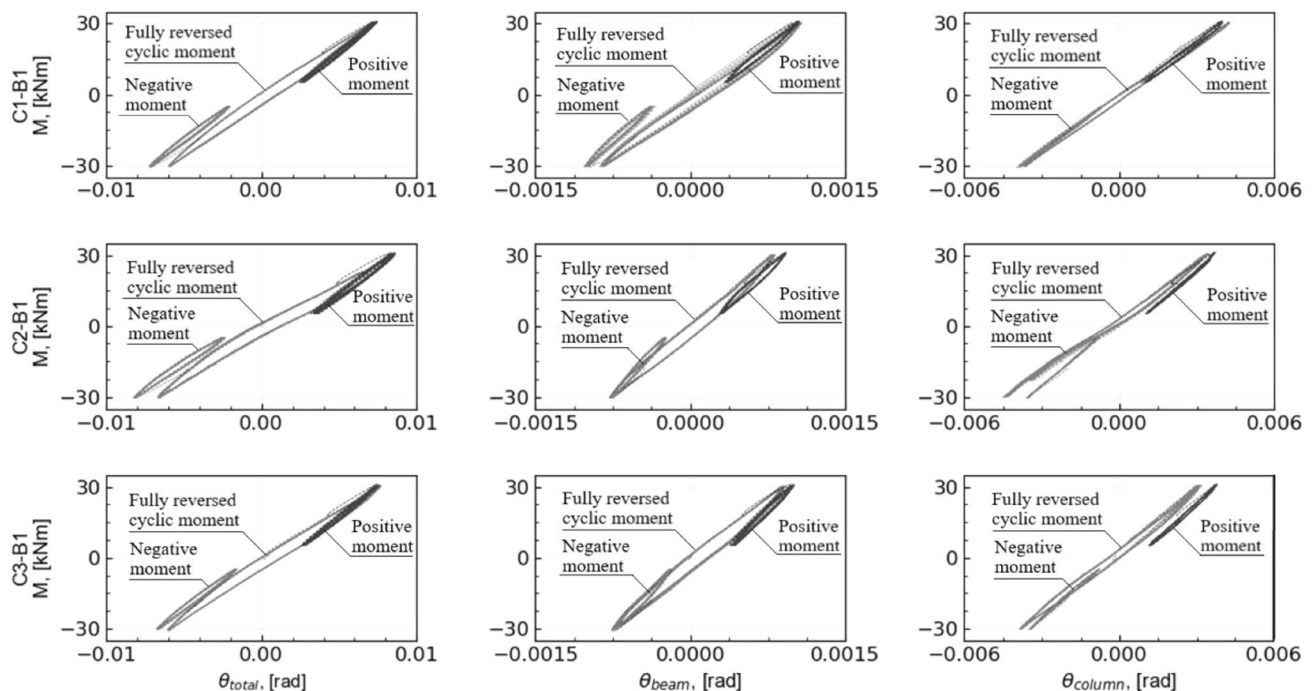

Fig. 7 Moment-rotation curves from cyclic tests of the connections

Table 4 Experimental results of connections subjected to cyclic testing

Entire connection

Test ID	Fully reversed cyclic			Negative moment			Positive moment		
	$K_{\theta,cyc}$, [kNm/rad]	E_d, [kNm]	ξ_{eq}, [%]	$K_{\theta,-}$, [kNm/rad]	E_d, [kNm]	ξ_{eq}, [%]	$K_{\theta,+}$, [kNm/rad]	E_d, [kNm]	ξ_{eq}, [%]
C1-B1	4465	0.052	4.1	4675	0.010	4.7	5028	0.010	4.7
C2-B1	3774	0.067	4.4	4090	0.014	5.5	4677	0.012	5.5
C3-B1	4287	0.054	4.1	4676	0.010	4.4	4993	0.008	3.8
Mean	4175	0.058	4.2	4480	0.011	4.9	4900	0.010	4.7
CoV, [%]	8.6	13.4	4.3	7.5	19.2	11.4	4.0	22.3	18.9

Beam-side connection

Test ID	Fully reversed cyclic			Negative moment			Positive moment		
	$K_{\theta,b,cyc}$, [kNm/rad]	E_d, [kNm]	ξ_{eq}, [%]	$K_{\theta,b,-}$, [kNm/rad]	E_d, [kNm]	ξ_{eq}, [%]	$K_{\theta,b,+}$, [kNm/rad]	E_d, [kNm]	ξ_{eq}, [%]
C1-B1	30,869	0.004	3.3	37,089	0.001	3.2	33,684	0.001	2.9
C2-B1	36,774	0.004	2.5	45,341	0.001	3.3	37,323	0.001	3.5
C3-B1	35,458	0.004	2.8	43,388	0.001	3.4	40,918	0.001	3.1
Mean	34,367	0.004	2.8	41,939	0.001	3.3	37,308	0.001	3.2
CoV, [%][a]	9.0	9.7	14.7	10.3	8.8	2.2	9.7	11.8	10.2

Column-side connection

Test ID	Fully reversed cyclic			Negative moment			Positive moment		
	$K_{\theta,c,cyc}$, [kNm/rad]	E_d, [kNm]	ξ_{eq}, [%]	$K_{\theta,c,-}$, [kNm/rad]	E_d, [kNm]	ξ_{eq}, [%]	$K_{\theta,c,+}$, [kNm/rad]	E_d, [kNm]	ξ_{eq}, [%]
C1-B1	8292	0.012	2.8	7500	0.003	2.2	7982	0.006	4.8
C2-B1	8567	0.017	2.0	8635	0.004	2.7	9106	0.004	3.6
C3-B1	8529	0.020	2.9	8887	0.003	2.3	9356	0.003	3.1
Mean	8463	0.016	2.6	8341	0.003	2.4	8815	0.005	3.8
CoV, [%]	1.8	22.8	19.0	8.9	27.6	10.2	8.3	29.9	22.9

values for lateral stiffness (K_{frame}), energy dissipation (E_d), viscous damping coefficient (ξ_{eq}), bending moments (M_c) and rotational stiffness of connections ($K_{\theta,y}$) are summarized in Table 5. Furthermore, the experimental results were compared with the FE model shown in Fig. 6a.

As shown in Table 5, the lateral stiffness of the mock-up frame assembly for loading in C_1, C_2, C_3 were measured to 2.43, 4.49, 2.33 kN/mm, respectively. The lateral stiffness is smallest when the load is applied on the corner columns, presumably due to torsion caused by the eccentric loading. Furthermore, the frame assembly showed considerable energy dissipation with equivalent viscous damping coefficients for all loading cases (3.11%, 2.62% and 4.65%).

3.2.2 Finite element evaluations

To examine the effects of the transversal (x-axis) rotational stiffness of the connections, a series of FE simulations of the frame assembly was carried out varying the ratio between the rotational stiffness about x-axis (transversal) and y-axis $K_{\theta,x}/K_{\theta,y}$. The rotational stiffness ($K_{\theta,y}$) about y-axis was fixed to 4200 and 2100 kNm/rad for centric and corner columns, respectively (i.e., the average rotational stiffness from the cyclic loading tests). The FE results are presented in Fig. 9 with corresponding lateral loading (F_{max}) on every column according to Table 5. The obtained displacements from FE simulations for all three columns were normalized with displacements of middle (C_2) column. The stiffness ratio range of $K_{\theta,x}/K_{\theta,y} = 0.2$–$0.3$, which is highlighted in Fig. 9, gives good agreement regardless of load condition and is valid both for static and dynamic response. The rotational stiffness of connection about x-axis does not affect horizontal displacements when the loading is applied on the centric column, confer Fig. 9. Furthermore, the mean rotational stiffness of connection measured in the laboratory was 4175 kNm/rad, but for the mock-up frame assembly the measurements gave rotational stiffness from 4166 to 4535 kNm/rad. The
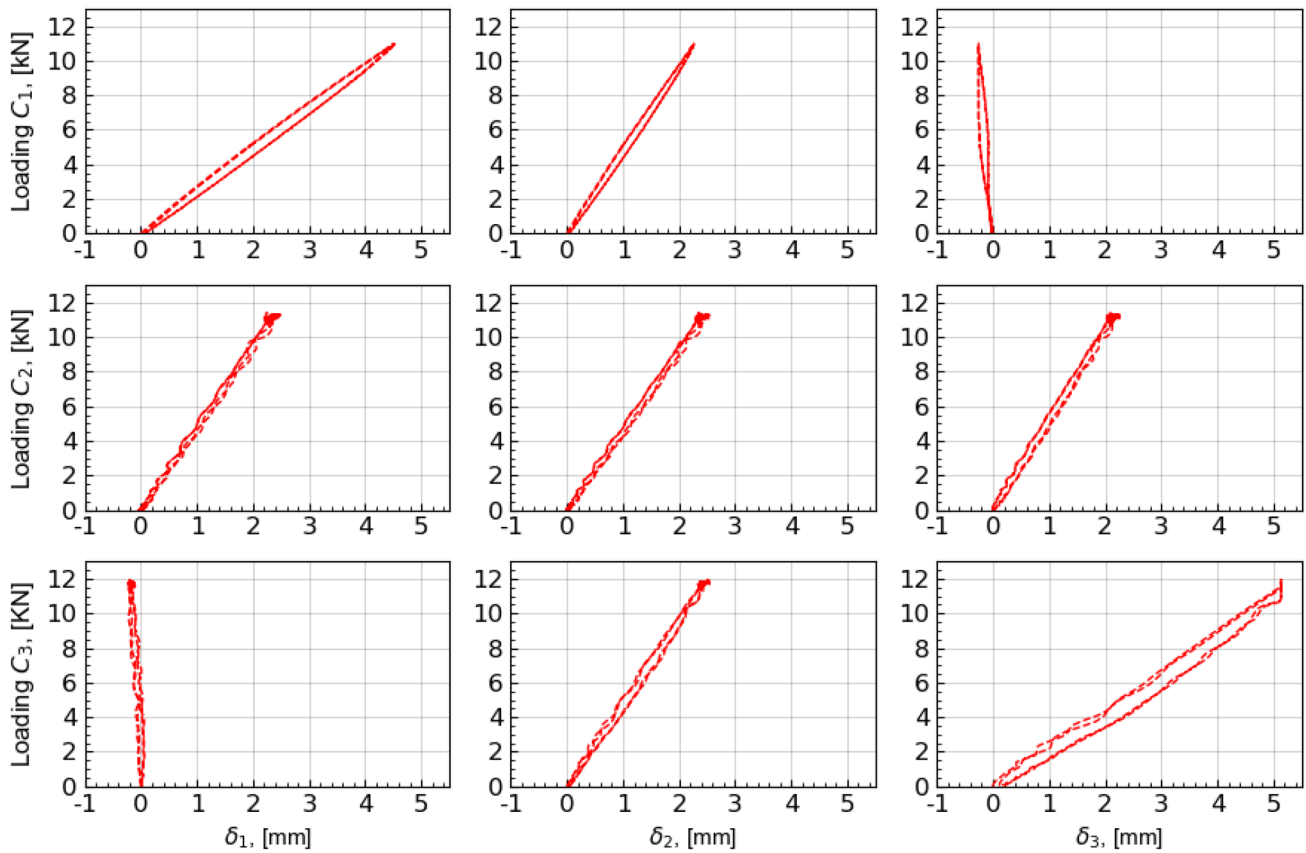
Fig. 8 Force–displacement curves from lateral cyclic tests of the mock-up frame assembly

Table 5 Experimental and FE results of mock-up frame assembly subjected to lateral cyclic loading

Property	Units	Loading C_1			Loading C_2			Loading C_3		
		C1	C2	C3	C1	C2	C3	C1	C2	C3
F_{max}	[kN]	11.00	–	–	–	11.40	–	–	–	12.00
K_{frame}	[kN/mm]	2.43	–	–	–	4.49	–	–	–	2.33
E_d	[kN]	2.46	–	–	–	1.15	–	–	–	4.53
ξ_{eq}	[%]	3.11	–	–	–	2.62	–	–	–	4.65
M_c [a]	[kNm]	5.30	5.03	0.36	2.63	5.10	2.63	0.42	5.48	5.73
M_c/θ	[kNm/rad]	1895	4535	2006	1822	4400	1932	1711	4166	1900
δ_{tests}	[mm]	4.52	2.27	–0.26	2.49	2.54	2.26	–0.26	2.55	5.14
δ_{FE} [a]	[mm]	5.26	2.46	–0.27	2.51	2.56	2.51	–0.30	2.68	5.73

[a]FE results assuming: $K_{\theta,y} = 4200$ kNm/rad, $K_{\theta,x} = 1184$ kNm/rad on centric columns and $K_{\theta,y} = 2100$ kNm/rad, $K_{\theta,x} = 592$ kNm/rad on corner columns

mean rotational stiffness of connection for corner columns was measured to 1878 kNm/rad. The FE model with the stiffness ratio $K_{\theta,x}/K_{\theta,y}$ in the range 0.20–0.30 also gave good agreement for the fundamental eigenfrequency in the y-direction compared to the experimentally obtained value of 1.81 Hz (Table 6), see the rightmost plot in Fig. 9. The corresponding vibrational modes from FE simulations are shown in Fig. 10.

3.2.3 Free damped vibration evaluation

The fundamental eigenfrequencies and damping ratios with respect to translation in x- and y-directions obtained from experimental modal analysis and FE simulation are given in Table 6. The fundamental eigenfrequency with EMA was recorded to be 1.81 Hz along the y-direction and 3.55 Hz along the x-direction with structural damping ratios of 2.1%
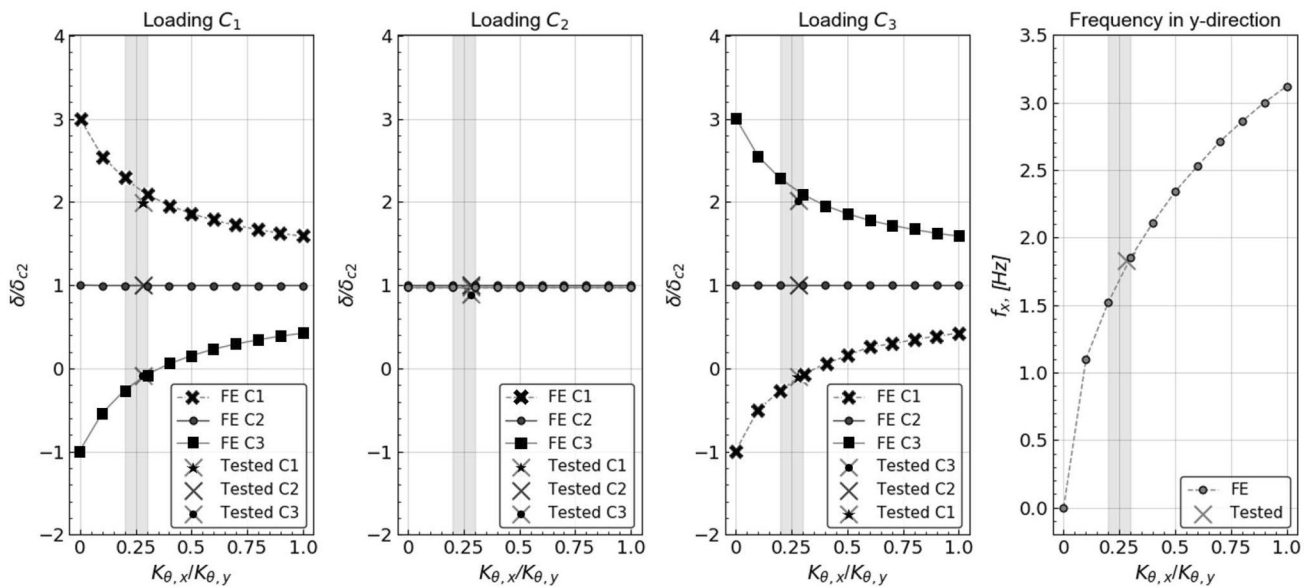
Fig. 9 Lateral displacements according to FE analyses of the frame assembly as a function of the ratio $K_{\theta,x}/K_{\theta,y}$

Table 6 Fundamental eigenfrequencies and structural damping from EMA and FE simulations

Test method	$f_{n,y}$, [Hz]	ξ_y, [%]	$f_{n,x}$, [Hz]	$\omega_{n,x}$,[rad/sec]	ξ_x, [%]
EMA	1.81	2.10	3.55	22.30	3.90
FE	1.80	-	3.34	20.98	3.88

and 3.9%, respectively. No experiment on energy dissipation in the connections for transverse direction (y-direction) was performed, and hence no comparison of FE and EMA is available for y-direction.

To evaluate the structural damping with FE simulations as discussed in Sect. 2.2.5, the material damping values of the timber columns and hollow box timber decks were applied. Additionally, the damping coefficients of the moment-resisting connections were estimated according to Eq. (35) and all values are presented in Table 7. The free damped vibration results from FE simulation are presented in Fig. 11 in terms of displacement vs time and compared with free damped vibration test results from values obtained with EMA by applying the equation of motion for damped structures:

$$u(t) = e^{-\xi_x\omega_{n,x}t}\left[u(0)\cos\omega_{d,x}t + \frac{\dot{u}(0) + \xi_x\omega_{n,x}u(0)}{\omega_{d,x}}\sin\omega_{d,x}t\right]$$

(37)
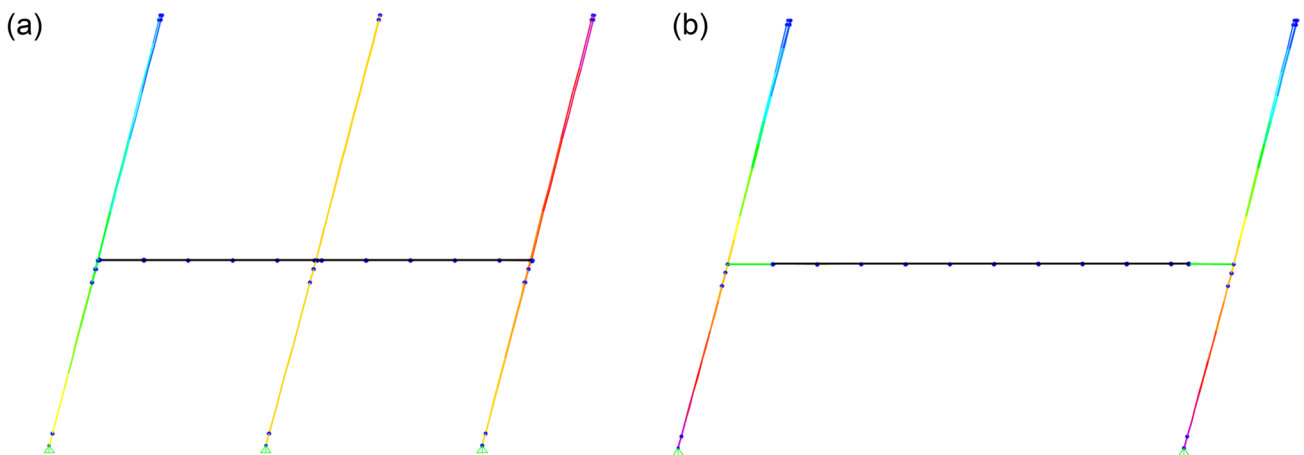
Fig. 10 Mock-up frame assembly mode shapes from FE software SAP2000: **a** First mode in transversal y-direction with frequency of 1.80 Hz; **b** Second mode in longitudinal x-direction with frequency of 3.34 Hz

Table 7 Material and equivalent viscous damping ratios for FE simulation

Structural part	Material damping, [%]	Equivalent viscous damping, [%]	Damping coefficient (c), [N × s/mm]
Timber columns	0.5	–	–
Hollow box timber decks	1.5	–	–
Moment-resisting connections on centric columns	–	4.2	16,816.0
Moment-resisting connections on corner columns	–	4.2	8408.0

FE simulations assuming: $K_{\theta,y} = 4200$ kNm/rad on centric columns and $K_{\theta,y} = 2100$ kNm/rad on corner columns. Undamped natural frequency $\omega_{n,x} = 2\pi \times f_{n,x} = 2\pi \times 3.34 = 20.98$ rad/s

$$\omega_{d,x} = \omega_{n,x}\sqrt{1 - \xi_x^2} \tag{38}$$

where ξ_x- is the structural damping from EMA, $\omega_{n,x}-$ is the natural frequency, $u(0)-$ is the initial displacement, $\omega_{d,x}-$ is the damped natural frequency, $\dot{u}(0)-$ is the initial velocity.

The initial displacement on the centric and corner columns at the level of hollow box timber decks $u(0) = 5.0$ mm and initial velocity $\dot{u}(0) = 0$ m/s were applied to measure free damped vibrations. The structural damping of FE frame assembly model according to Eq. (36) and Fig. 11 is 3.88%.

As can be seen in Table 6, as well as Fig. 11, a minor difference in the fundamental frequency $f_{n,x}$ between the FE model (with measured component values) and the EMA results (of the mock-up frame assembly) is present. The FE model gives $f_{n,x} = 3.34$ Hz, while $f_{n,x} = 3.55$ Hz is obtained

from EMA. This is probably due to small differences in the rotational stiffness of the connections. The resulting deviation in frequency is consistent with the fact that the connection stiffness obtained from the mock-up (and consequently in the EMA) were slightly larger than the stiffness measured in the connection component tests. It should also be kept in mind that there are experimental variations in the performance of the connections, both in the component tests as well as in the mock-up frame assembly tests. The use of material damping and equivalent viscous damping from the cyclic connection tests show very good agreement, and this approach can successfully be used to predict the structural damping of complete frame assemblies.

4 Conclusion

The performance of beam-to-column moment-resisting timber connections with inclined threaded rods and steel coupling parts connected with friction bolts has been investigated by use of full-scale tests and a mock-up frame assembly. The moment resisting connections were subjected both to cyclic and monotonic loading. The rotational stiffness and the energy dissipation properties were determined on the basis of three full-scale cyclic tests. In addition, the rotational stiffness and the moment resistance were measured under monotonic loading and compared with analytical predictions based on an analytical model (Stamatopoulos and Malo 2020a). The mock-up frame assembly was subjected to cyclic lateral loading and also tested with experimental modal analysis. The lateral stiffness, energy dissipation, fundamental eigenfrequencies and structural damping of the frame assembly were measured and quantified and compared with FE analyses. The following main conclusions are drawn:

Fig. 11 EMA and FE free damped vibration results in x-direction
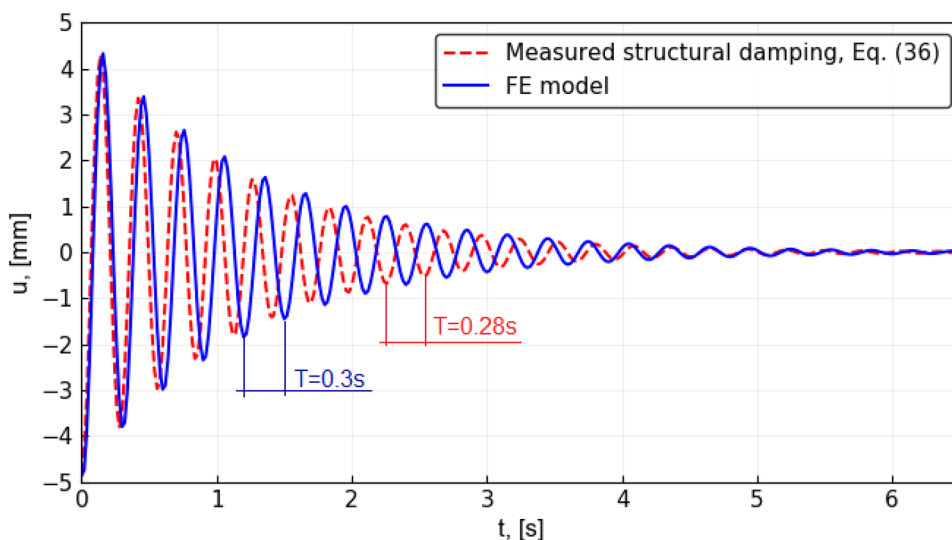
- The rotational stiffness of present connection measured from monotonic loading test was 4761 kNm/rad. The maximum moment resistance was 100.6 kNm limited by friction between the steel plates. No initial slip was recorded, and the connection demonstrated initial load take-up.
- The rotational stiffness of connections for fully reversed loading and single-sided positive and negative moment tests were 4175, 4480 and 4900 kNm/rad, respectively. The coefficient of variation of stiffness values is from 4.0 to 8.6%, and hence, only minor differences are exhibited by this type of connection.
- The mean rotational stiffness of connection from laboratory tests and from tests with mock-up frame assembly was on average 4175 kNm/rad and 4367 kNm/rad, respectively. Therefore, the measured values for connection properties obtained in the laboratory are also achievable in full-scale assemblies for this type of connection.
- The rotational stiffness of connections obtained from fully reversed cyclic loading tests are very suitable for FE simulations. The FE model shows good agreement between the experimental results and the analytical model.
- For unsymmetrical loading conditions when torsional rotation of the frame assembly is introduced, the transversal rotational stiffness of the connections should be considered. The transversal rotational stiffness value of these moment-resisting connections can be assumed to be around 0.20–0.30 $K_{\theta,y}$.
- The moment-resisting connections and mock-up frame assembly tests under cyclic loading showed high-energy dissipation; 4.2% and 3.5% in terms of equivalent viscous damping, respectively.
- Cyclic energy dissipation from quasi-static component tests can be used to predict the structural damping in moment-resisting frames. Provided that the amount of material damping is known in the components, the damping caused by the connections can be modelled by equivalent viscous damping in FE models, and consequently the structural damping in framed structures can be predicted.

Authors' contributions AV has written the paper (including figure preparation), performed all experimental static tests of the moment-resisting connections and mock-up frame assembly, Finite Element simulations and performed all calculations. AV, SØN contributed to the mock-up frame assembly process. SØN has performed experimental modal analysis of the mock-up-frame assembly. HS, KAM have contributed to the concept/content development and have critically reviewed the manuscript. The 1st authors have developed the original concept of steel coupling part based on L-profiles and friction bolts. KAM has developed the conceptual design of the experimental protocol and energy dissipation determination and has developed the original concept of moment-resisting beam-to-column connections based on inclined threaded rods. HS has developed the component method and derived the analytical equations. All authors have seen and approved the manuscript and have contributed significantly to its preparation.

Declarations

Conflict of interest On behalf of all authors, the corresponding author states that there is no conflict of interest.

References

Andreolli M, Piazza M, Tomasi R, Zandonini R (2011) Ductile moment-resistant steel–timber connections. Proc Inst Civ Eng Struct Build 164(2):65–78

Brandon D, Leijten A (2014) Structural performance and advantages of DVW reinforced moment transmitting timber joints with steel plate connectors and tube fasteners. In: Materials and joints in timber structures. Springer, New York, pp 255–263

Buchanan A, Deam B, Fragiacomo M, Pampanin S, Palermo A (2008) Multi-storey prestressed timber buildings in New Zealand. Struct Eng Int 18(2):166–173

Chopra AK (2012) Dynamics of structures: theory and applications to earthquake engineering. 4th edn. Upper Saddle River, N.J.: Prentice Hall

Conta S, Homb A (2020) Sound radiation of hollow box timber floors under impact excitation: An experimental parameter study. Appl Acoust 161:107190

Dassault Systemes Simulia Corp (2014) Abaqus analysis user's guide. Version 6:14

European Committee for Standardization (1991) EN 26891:1991: Timber structures- Joints made with mechanical fasteners-General principles for the determination of strength and deformation characteristics. Belgium, Brussels

European Committee for Standardization (2010) NS-EN 1995-1-1:2004+A1:2008+NA:2010, Design of timber structures - Part 1–1: General - Common rules and rules for buildings. Belgium, Brussels

European Committee for Standardization (2013) EN 14080–2013: Timber structures- Glued laminated timber and glued solid timber - Requirements. Belgium, Brussels

Gohlich R, Erochko J, Woods JE (2018) Experimental testing and numerical modelling of a heavy timber moment-resisting frame with ductile steel links. Earthq Eng Struct Dyn 47(6):1460–1477

Kasal B, Guindos P, Polocoser T, Heiduschke A, Urushadze S, Pospisil S (2014) Heavy laminated timber frames with rigid three-dimensional beam-to-column connections. J Perform Constr Facil 28(6):A4014014. https://doi.org/10.1061/(ASCE)CF.1943-5509.0000594

Komatsu K, Teng Q, Li Z, Zhang X, Que Z (2019) Experimental and analytical investigation on the nonlinear behaviors of glulam moment-resisting joints composed of inclined self-tapping screws with steel side plates. Adv Struct Eng 22(15):3190–3206

Kristoffersen T, Bjørge H (2017) Konseptstudie av trebaserte komposittdekker med mulighet for innspenning til limtresøyler. (Conceptual studies of wood based floor with semi-rigid supports). NTNU

Labonnote N, Rønnquist A, Malo KA (2013) Experimental evaluations of material damping in timber beams of structural dimensions. Wood Sci Technol 47(5):1033–1050

Lam F, Gehloff M, Closen M (2010) Moment-resisting bolted timber connections. Proc Inst Civ Eng Struct Build 163(4):267–274

Leimcke J, Rüther N, Guindos P, Brunnermeier M (2016) Moment connection with frictional damping for timber post and beam construction in earthquake-prone areas. 22. Internationales Holzbau-Forum IHF

Lied K, Nordal K (2016) A conceptual study of glulam connections using threaded rods and connecting circular steel profiles. MSc thesis, NTNU Norwegian University of Science and Technology

Malo K A, Köhler J (2013) Vibrations of timber floor beams with end restraints, structures and architecture: concepts, applications and challenges. In: Proceedings of the 2nd International Conference on Structures and Architecture, ICSA 2013, pp 181–189

Oskouei R, Chakherlou T (2009) Reduction in clamping force due to applied longitudinal load to aerospace structural bolted plates. Aerosp Sci Technol 13(6):325–330

Qazi J (2020) Embedment strength and stiffness of threaded rods in softwood (in Norwegian). MSc thesis, NTNU Norwegian University of Science and Technology

SAP2000 Analysis reference manual, Computers and Structures, Inc., Berkley, California, USA, 2003.

Solarino F, Giresini L, Chang W-S, Huang H (2017) Experimental tests on a dowel-type timber connection and validation of numerical models. Buildings 7(4):116

Stamatopoulos H, Malo K A (2020a) Analysis of moment-resisting beam-to-column timber connections with screwed-in threaded rods. WOODSOL internal report

Stamatopoulos H, Malo KA (2020b) On strength and stiffness of screwed-in threaded rods embedded in softwood. Constr Build Mater 261:119999

Vilguts A, Stamatopoulos H, Malo KA (2020) Parametric analyses and feasibility study of moment-resisting timber frames under service load. Eng Struct 228:111583

Vilguts A, Malo KA, Stamatopoulos H (2018) Moment resisting frames and connections using threaded rods in beam-to column timber joints. In: Proceedings of WCTE 2018 - World Conference on Timber Engineering. Seoul, Republic of Korea

Wilson EL, Habibullah A (1997) SAP2000 integrated finite element analysis and design of structures. Computers and Structures Inc., Berkeley, California